Instrument Science Report 2017-13

Generating the WFC3 UVIS Post-Flash Reference File

H. Kurtz
S. Baggett

June 2, 2017

Abstract

We have created and delivered new post-flash reference files for the WFC3 UVIS channel. The files are generated from stacks of high signal-to-noise data taken from 2012-2016 (proposals 13560, 13568, 14372, 14006, 13069, 13078), about 220 images in all. Each frame was post-flashed for 100 sec at medium current yielding ∼7000 e-/pixel background per image. The reference files are scaled down to the equivalent of 1 sec of post-flash; the calibration software calwf3 rescales them to match the post-flash level used in the science image. Calibration reference files for unbinned data, for both shutter A and B, and for the low and medium current settings have been delivered. The overall output of the LED shows a slow long-term decline of about 0.17% per year, with random image-to-image variations of up to ∼0.5%. We confirm the illumination pattern is the same as previously measured: shutter B is 0.6% fainter than shutter A and the shutter A to shutter B ratio shows a gradient of ∼4% . The new post-flash reference files will be available in the pipeline software version 2017_2, recorded in the OPUS_VER header keyword.

Introduction

All past and present CCDs on HST show charge transfer efficiency (CTE) degradation due to the harsh on-orbit radiation environment. These traps arise due to the bombardment of the detector by cosmic rays which generate charge traps in the detector material. The traps can rob images of electrons during the readout process. The further the source signal

packet is from the readout amplifiers, the more traps it encounters, thus the higher the charge losses. In addition, the traps grow in number over time, further increasing the losses. Given enough traps, the signal from faint targets can potentially be lost completely. One mitigation strategy against CTE loss is to increase the background of the image before it is read out; this fills the traps so that charge packets travel to the amplifiers with less interference and consequently fewer losses. In order to raise the background in images which do not have sufficient natural sky background, WFC3 has a post-flash capability that on-orbit tests have shown is highly effective in reducing CTE losses (Anderson, et al., 2012).

The WFC3 post-flash mechanism consists of an LED that illuminates the backside of the shutter just prior to the image readout. The diffuse light adds a repeatable and relatively uniform background (±20%) to the data (Baggett and Wheeler, 2012). Past analysis has shown that the illumination pattern differs slightly between the two shutters: shutter B is 0.6% fainter than shutter A and the shutter A to shutter B ratio shows a gradient of ∼4% (Biretta and Baggett, 2013). For the WFC3 CCDs, the 'sweet-spot' to best reduce the CTE losses without adding too much additional shot noise is a ∼12 e-/pixel total background (natural + flash) (Anderson, et al., 2012). With such a background, CTE losses for a low signal-to-noise ratio object are reduced from 90% to 15% (Anderson, et al., 2012; Gosmeyer and Baggett, 2017). Further improvements can be obtained by using the pixel-based CTE corrected data products (extension flc), now a standard output of the calibration pipeline (Russell et al., 2016). The available phase II post-flash levels are shown in Table 1 along with the current setting and lamp flash duration required to achieve that level (reproduced from Biretta and Baggett, 2013). Note that observers need only specify the desired post-flash level in electrons (e-) in their APT proposal file; the scheduling software employs a look-up table to determine the flash current and duration required to achieve that level.

Since the flash is not part of the "real" data, i.e. the science scene, it must be removed from the image. This is done in the calibration pipeline by subtracting a post-flash reference file (Deustua, S ed. 2016). In this report, we summarize the properties of the post-flash and describe the creation of the new post-flash reference files. We also evaluate the performance and usage of the post-flash over time.

Post-Flash Data

The new post-flash reference files presented in this report were created from data observed between 2012-2016 (proposals 13560, 13568, 14372, 14006, 13069, 13078). Once a month four full-frame post-flash images are taken, two per shutter. Once a year we take about 12 full-frame images on the same day (6 per shutter). A total of about 220 images (110 per shutter) were combined to create the reference files. The instrument's flight software can not post-flash 0 sec bias frames so the calibration observations are the shortest possible dark frames (0.5 second). These short darks receive a 100 sec medium current post-flash resulting in about 7000 e-/pixel background and a total exposure duration of 100.5 seconds (time used for the dark correction).

Figure 1 is a median image of 111 post-flash files taken with 100 sec post-flash at the medium current setting (header keywords FLASHDUR=100 and FLASHCUR=MED, respectively). This file will become the reference file at a later stage.

Phase II post-lash level (e-/pixel)	Lamp flash duration (sec)	Lamp current
1	0.4	LOW
2	0.8	LOW
3	1.2	LOW
4	1.6	LOW
5	2.0	LOW
6	2.3	LOW
7	2.7	LOW
8	3.1	LOW
9	3.5	LOW
10	3.9	LOW
11	4.3	LOW
12	4.7	LOW
13	5.0	LOW
14	5.4	LOW
15	0.2	MEDIUM
16	6.2	LOW
17	6.6	LOW
18	7.0	LOW
19	7.3	LOW
20	7.7	LOW
21	8.1	LOW
22	0.3	MEDIUM
23	8.9	LOW
24	9.3	LOW
25	9.7	LOW

Table 1: Phase II post-flash levels

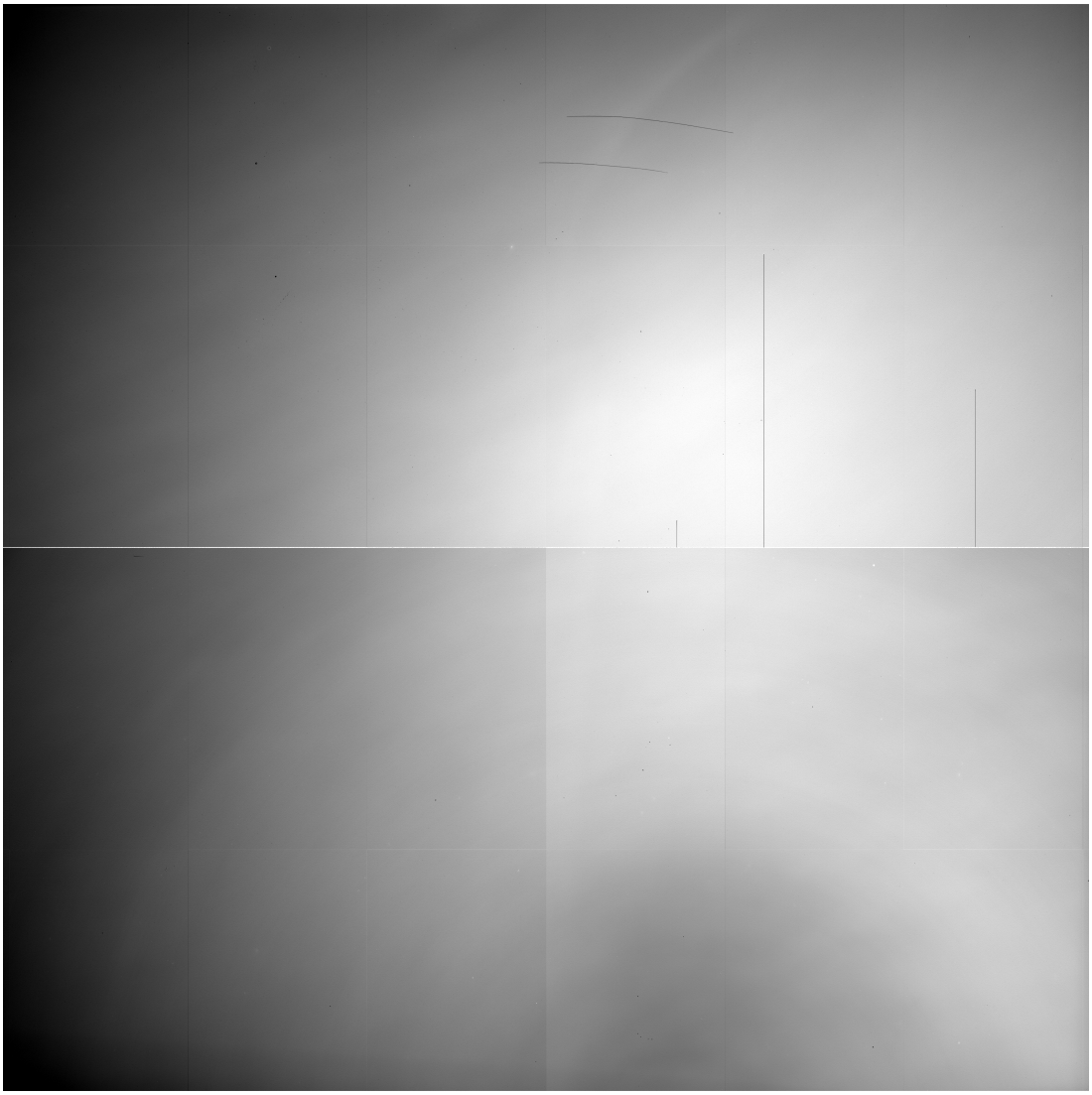

Figure 1: Median full-frame image for shutter A, medium current, 100 second post-flash. Greyscale is ±5% . Quadrants A,B,C,D are at upper left, upper right, lower left, and lower right, respectively.

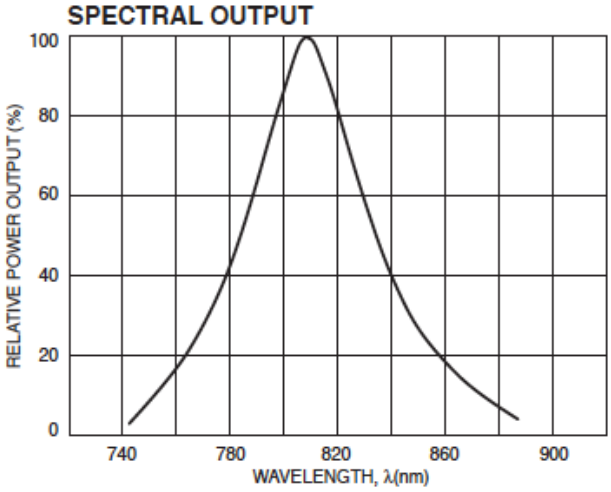

Figure 2: Output of the post-flash LED versus wavelength (OptoDiode Optoelectronics Data Book (2015)).

General Properties of Post-Flash

As seen in Figure 1, the post-flash illumination pattern is relatively smooth, varying by $\pm 20\%$ across the field of view. The peak illumination falls on the right quadrants (B and D) with a roll-off in illumination level towards the left edge of the field of view. Also visible in the image, in quadrant B, are several bad partial columns and two nearly horizontal scratches. Fainter grid lines, spaced about every 700 columns and every 1000 rows, are lithographic features, an artifact of the manufacturing process (these features do cause small-scale astrometric errors but are correctable e.g. Platais 2014).

No Fringing Detected

We examine the median combined post-flash as well as individual post-flash images and found no evidence of fringing.

A fringe model is developed from the LED spectra 2 (OptoDiode Optoelectronics Data Book (2015)) and is compared to the post-flash data. The LED has a wide range of wavelengths $\sim 740 - 880$nm. The fringe model is created using the software developed in Wong 2010. The software requires the source (LED) spectral energy distribution and the filter through put (in this case no filter).

We use this model in an attempt to remove fringing from the post-flash. The post-flash files are put through the fringe removal process described in Kurtz et al. 2017. No fringing was detected in the post-flash images. We confirm these results by examining the column mean of the fringe and the post-flash images. The column mean was calculated both across the whole image and in sections where we expect the worst fringing would appear. Figure 3 shows the locations of the sections plotted, the plot of the means of the fringe model

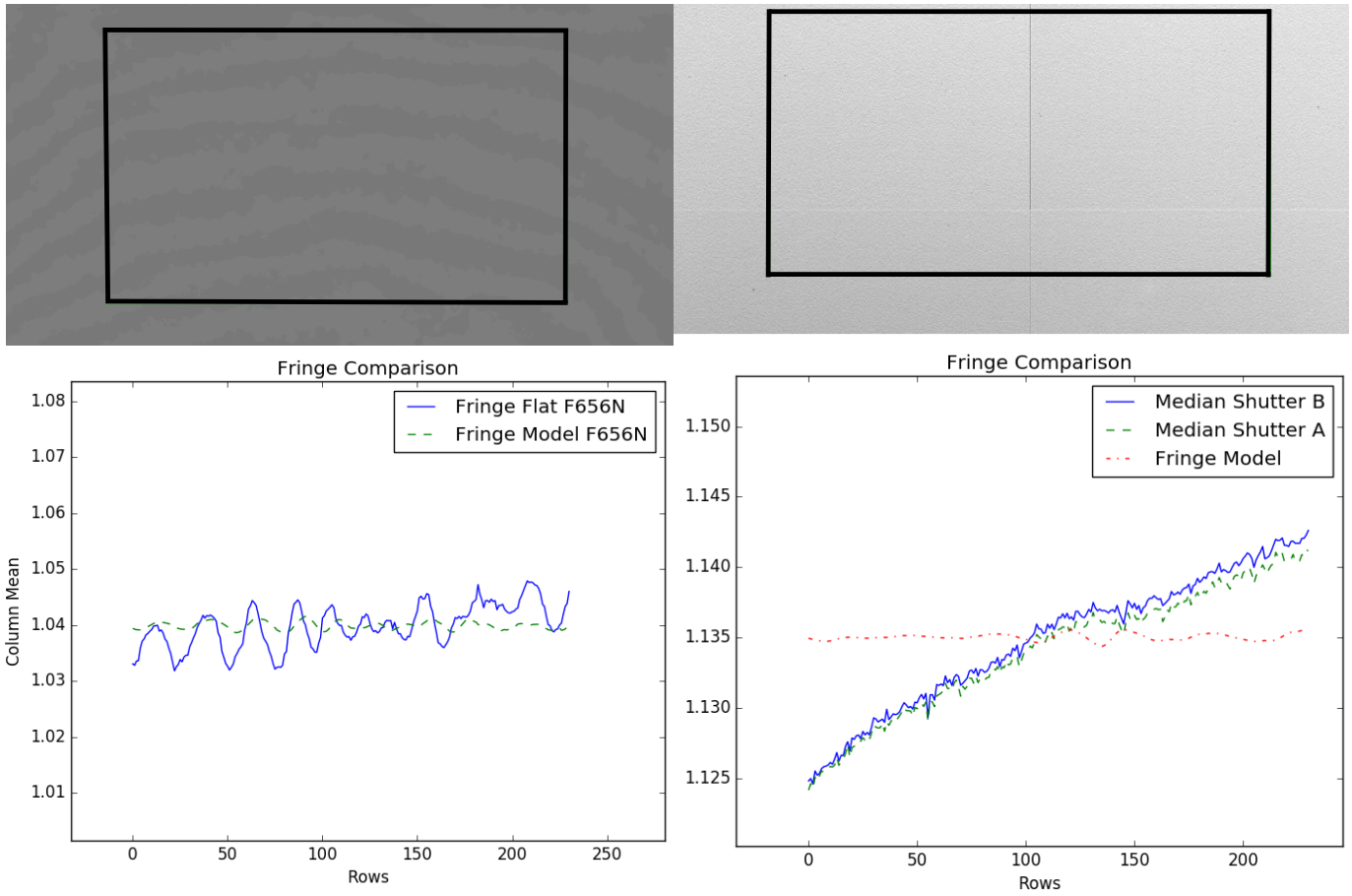

Figure 3: The top two panels are sections of the fringe model(left) and the median combined post-flash for shutter B(right). The scales of the images are +/- 0.2% and +/- 0.5% respectively. The box outlines the section used in creating the lower plots. The left plot is an example of our fringe model and corresponding flat field for F656N. The right plot is the column averages for the fringe model(red dash and dot line), median combined post-flash shutter A and B(green dashed line and blue solid line respectively).

compared to those of the post-flash for shutter A and B, as well as an example of the fringe model compared to a flat in the 656 narrowband filter. It is apparent in the top images of Figure 3 that fringing is not visibly detected, which is confirmed in the plots below. The left plot showing the F656N model compared to a flat and the right showing the post-flash compared to the LED model. The plot of the LED model compared to the post-flash shows that the fringe model is not observed as it it in the F656N plot.

Shutter Variations

As previously described, the post-flash is performed with an LED that illuminates the CCD before readout. The LED light is reflected off one of two shutters, A or B. Each shutter is unique due to variations during manufacture (finish, paint, etc.), thus, each can be expected to reflect the LED light slightly differently. With that in mind we make separate reference files for each shutter. A comparison of the resulting files shows that post-flash using shutter A is ∼6% brighter than on shutter B. The ratio of shutter A to shutter B post-flash illumination is relatively flat as shown in Figure 4. There is a shallow gradient from the upper left (amplifier A, about 1.077) to the lower right (amplifier D, about 1.057). The overall average of the ratio of shutter A to shutter B is 1.067 across the whole field with a standard deviation of 0.009. These values are consistent with earlier post-flash analysis results (Biretta and Baggett (2013)).

Post-Flash Stability

The routine monitoring of the LED stability is performed by taking relatively frequent images in the UVIS2-C1K1C-SUB aperture, a 1024x1024 pixel subarray, which is in the bottom left corner of the field of view close to amplifier C. The subarray format maximizes the number of levels that can be sampled in a given orbit while keeping total on-orbit calibration time required for monitoring at a minimum. That study, based on about 650 subarray images, found an average long-term decline in LED output of ∼0.15% per year ±0.24% as well as occasional short-term deviations from image to image of order a few % (C. Martlin 2017).

We take the opportunity with our high signal-to-noise full-frame images to examine the stability of the LED across the full field of view though at a significantly reduced cadence compared to the subarray study. Figure 5 plots the normalized averages of full-frame post-flash images taken at three epochs spanning over three years on shutter A. The orange stars are data taken on the same day in 2013, the red triangles are data from 2014, and the yellow squares are the 2015 data. Each year has at least 6 images taken on the same day; the blue circles are the averages for each day. The solid blue line plots the best fit of the average of each day and the green dashed line is the best fit to the individual images. Based on this relatively small set of images, the average output level has decreased by ∼0.3% per year. The spread on each day is ∼0.5% which is consistent with the scatter observed in the standard LED monitor program using subarrays (C. Martlin, 2017). This daily spread is time-independent, i.e. there are no short-term trends between LED output and the observation start time. Shutter B data show the same behavior.

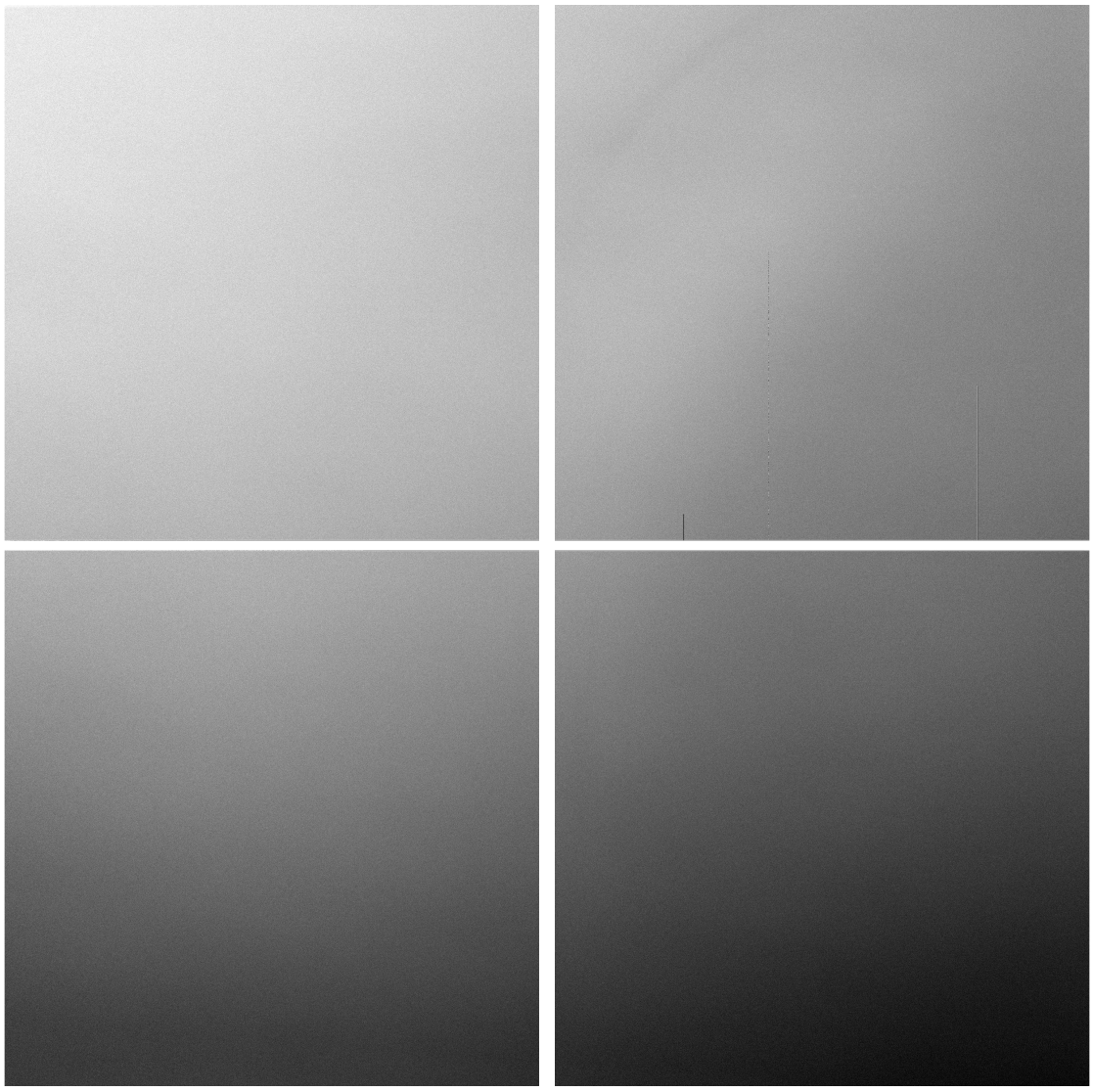

Figure 4: Low current reference file ratio shutter A/shutter B. This is a full-frame image with amplifier A, B, C, and D, in the upper left, upper right, lower left and lower right, respectively. Greyscale is ∼1.5%.

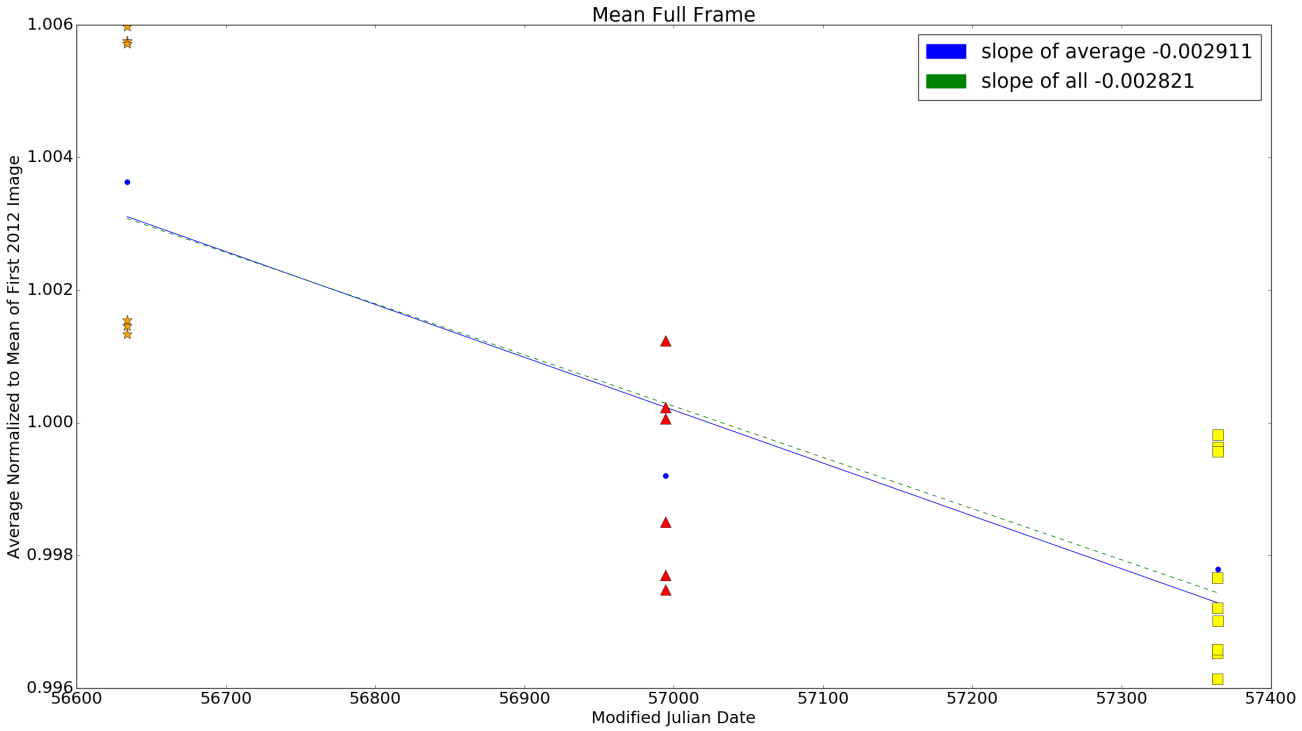

Figure 5: Normalized averages of high signal-to-noise full-frame post-flash images on shutter A as a function of observation date: orange stars for 2013, red triangles for 2014, and yellow squares for 2015. The large blue circles are averages of the yearly image sets. The y-axis is normalized to the value of the first post-flash image taken on August 27, 2012.

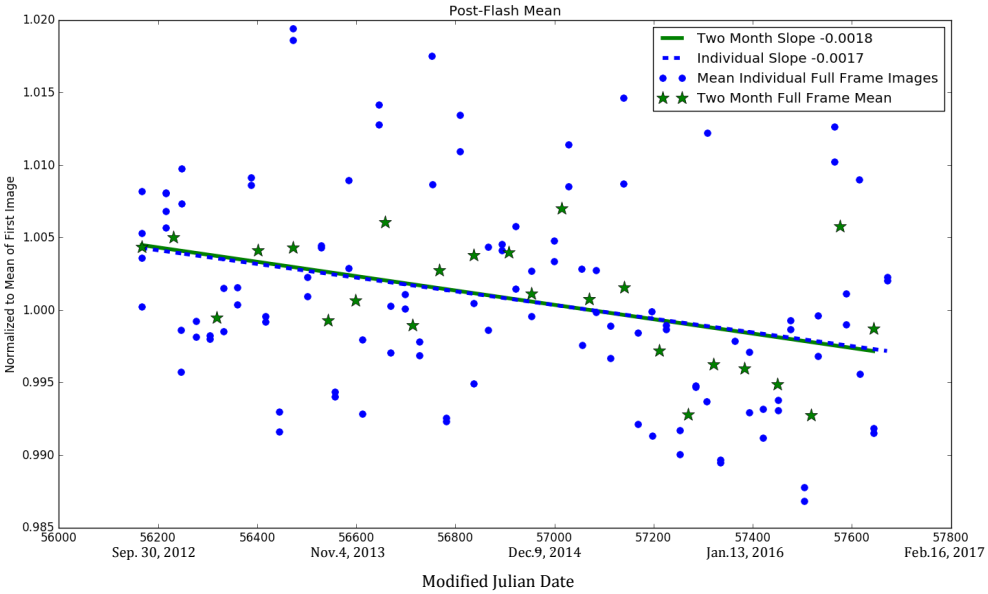

Figure 6: Illumination level of shutter A images, blue dots for individual images and green stars for 2-month averages.

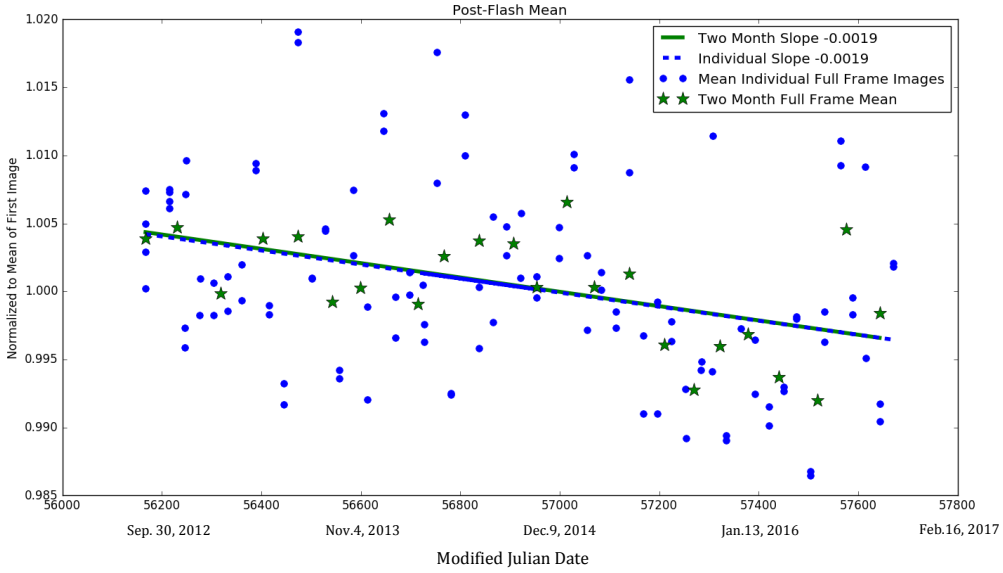

Figure 7: Illumination level of shutter B images, blue dots for individual images and green stars for 2-month averages.

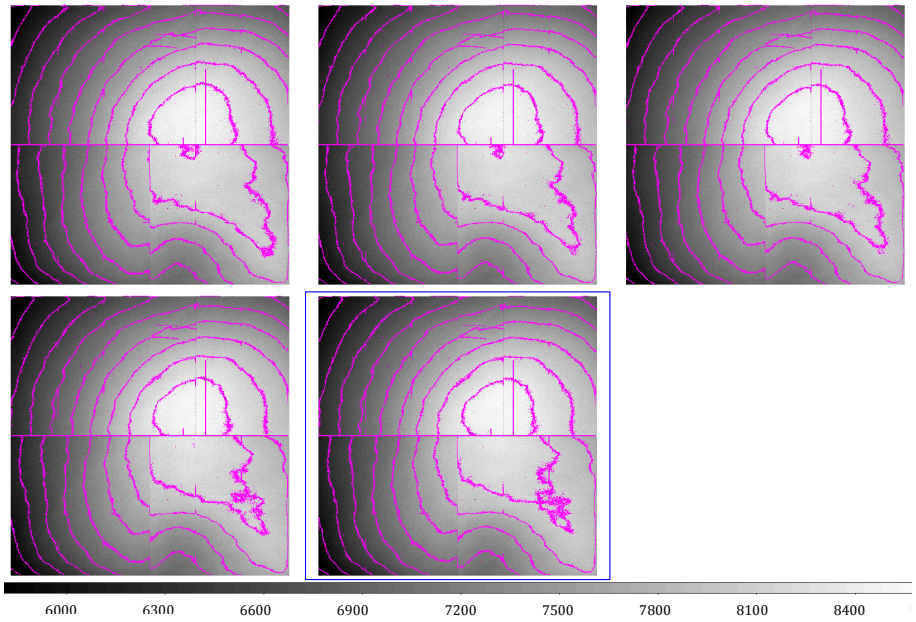

Figure 8: Contour plots of the yearly image stacks for shutter A. The 2012, 2013, and 2014 images are in the upper left, center, and right, respectively while 2015 and 2016 are in the lower left and lower right. Contours are plotted from 5700 to 8700 electrons in intervals of 300 electrons. The discontinuity in the contours at the quadrant boundaries due to slight differences in the gains of the amplifiers.

Similar trends are seen when we plot the statistics for all the full-frame high signal-to-noise individual images, as shown in Figure 6 and Figure 7. The individual averages of the medium post-flash images are the blue circles; the blue solid line corresponds to the fit to these individual points. The green stars are the averages of groups of two months of data; the green dashed line is the line of best fit for the grouped data. There is a slight decrease in LED output over time, 0.17% per year for shutter A and 0.19% per year for shutter B.

Finally, we investigate the behavior of the post-flash illumination pattern of over time. We group the images by year and generate median stacks. Table 2 summarizes the statistics of the median combined images. Contour plots are shown in Figure 8 and Figure 9 for shutters A and B, respectively; contours range from 5700 to 8700 electrons in intervals of 300 electrons. The structure and shape of the image contours remains largely the same, however some slight shifts are apparent. The subtle changes are easiest to detect in the outer left corners, where the LED light is rolling off slightly i.e. the contours are more closely spaced. The 2012 full-frame image stack is on average 0.7% brighter than the 2016 combined image, in rough agreement with the output decline observed in the subarray study (C. Martlin, 2017). Given the change is less than 1%, we do not generate time-dependent post-flash reference files. However, if the LED decline continues, future updates will include epoch-based reference files.

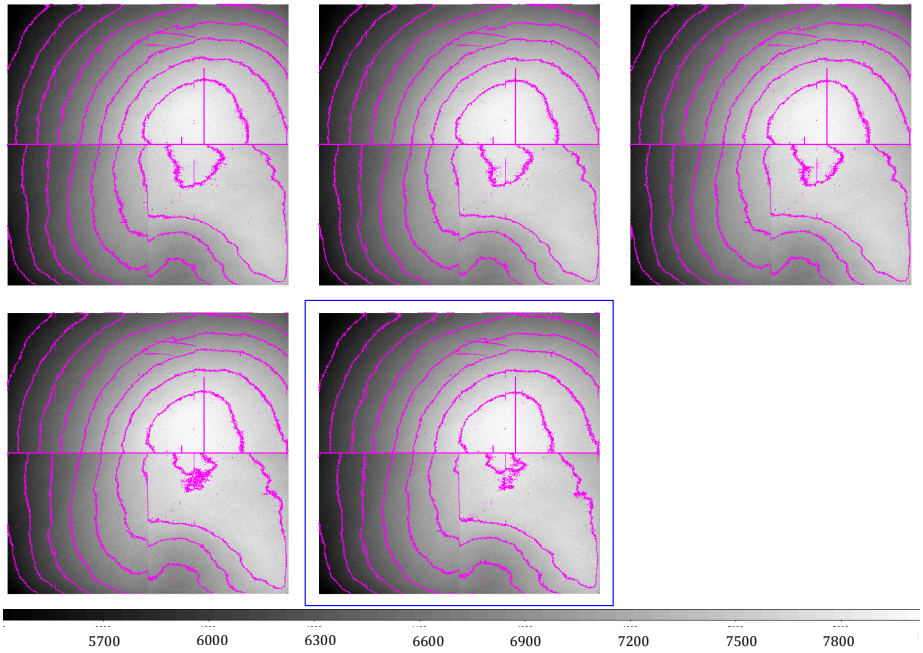

Figure 9: Same as for Figure 7 but for shutter B.

Shutter A

Year	Mean	Standard deviation	Normalized mean	Number of images
2012	7475.9	0.06	1.000	14
2013	7463.4	0.06	0.998	26
2014	7462.1	0.06	0.998	24
2015	7438.4	0.06	0.995	25
2016	7427.8	0.06	0.994	22

Shutter B

Year	Mean	Standard deviation	Normalized mean	Number of images
2012	7010.1	0.06	1.000	14
2013	6999.5	0.06	0.998	26
2014	6995.8	0.06	0.998	25
2015	6974.2	0.06	0.995	25
2016	6963.4	0.06	0.993	22

Table 2: Statistics of the yearly combined post-flash files, normalized to 2012 data.

	Low current	Medium current	High current	Total
Number of Images	26305	1140	10	27455
Time on in Hours	31.01	9.149	0.003	40.16

Table 3: The lifetime usage of the post-flash LED. (As of May 1, 2017)

LED Usage

We summarize the on-orbit usage of the LED in Table 3. Note that not all UVIS images require a post flash e.g. if the natural background of an image is 12 electrons per pixel, a post-flash is unnecessary and the post-flash was first implemented on-orbit in 2012, about 3 years into the mission. As of May 1,2017, the total number of post-flashed images is 27455, out of about 93000 total on-orbit UVIS images in the archive.

The LED has been on for a total of about 40.16 hours as of May 1, 2017, an extremely tiny fraction of the expected LED lifetime of 100,000 hours. There is also a second spare LED on board WFC3, however it only operates from the other electronics box and would require an instrument side-switch. We separate the lamp on-time by the LED current levels (high, medium, and low). The high current post-flash, only about 12% brighter than the medium current (Biretta and Baggett (2013)), is rarely used and then, only for testing purposes, not for science data.

Creation of Low Current Un-binned Reference File

As previously discussed, the post-flash illumination pattern of the two shutters differs by ∼6% therefore separate reference files are implemented for each shutter. The LED illumination behavior is stable enough that we generate a single post-flash reference file for each shutter setting. Time-dependent files may be implemented in the future if the LED level continues to drop (Figure 5). The procedure to generate the reference files includes calibrating the images using calwf3 version 3.3 (e.g. bias level, dark correction), performing cosmic ray rejection, stacking the images, vetting the results, formatting the files for use by the calibration software, and finally delivering and installing them into the calibration reference file system for use in the pipeline.

We create association tables for the individual images and feed them to calwf3 to perform the calibrations and flag cosmic rays. We median combine the calibrated, CR-clean images, masking any pixel flagged in the DQ file i.e. any pixels with a value greater than zero in the DQ array. There are a total of 111 and 112 images, in the resulting Shutter A and B reference files, respectively.

The combined stacked image is then scaled to an equivalent one second low current post-flash, the format required by the calibration pipeline. The images that are combined are 100 second flash-duration images thus we divide by that exposure time. To convert from medium to low current, we multiply by the scale factor 0.03639 (Biretta and Baggett (2013)). The scaling is based on a sigma-clipped (3 x 2 sigma) ratio of a one second low current image stack to a one second medium current image stack. The value for the scaling that we compute from our data is 0.036392, in excellent agreement with the factor determined previously.

Finally, we populate the error arrays by propagating the errors in quadrature into the final reference files.

Creation of Medium Current Un-binned Reference File

In order to create the medium current reference file for the calibration pipeline, we re-scaled the low current reference file. We do not simply use the medium current image stack as-is because that is generated from long flash duration data; rescaling the low current file to a medium equivalent provides a reference file appropriate for the short flash-durations used for science data. For the scale factor we use 28.96 as determined by Biretta and Baggett (2013), generated from the ratio of a Flash 15/ Flash 12 exposure multiplied by the ratio of their respective exposure times (4.7/0.2).

Conclusions and Future Work

We use high signal-to-noise post-flash data from 2012-2016 (proposals 13560, 13568, 14372, 14006, 13069, 13078) to generate new post-flash reference files, one for each shutter. These files are in use in the automated calibration pipeline as of version 2017_2 (recorded in the image header keyword OPUS_VER). Observers with post-flashed science data processed prior to 2018_2 may obtain recalibrated versions by requesting their datasets from MAST (Mikulski Archive for Space Telescopes).

In agreement with previous studies, we find that the shutter A reference file is somewhat (6%) brighter than shutter B, primarily due to an illumination level offset as the image ratio of shutter A/shutter B is relatively smooth. The short-term LED output appears to be relatively stable, varying by at most about 0.5% from image to image. There does appear to be a low-level long-term dimming by about 0.17% per year and the illumination level contour levels, especially near the left edge of the FOV, are changing slightly. If those trends continue, it will become necessary to install time-dependent post-flash reference files.

Other future improvements could involve investigation of the non-linearity of LED output as a function of flash duration. The reference file has been calibrated for a FLASH level of 12; flashes that are significantly brighter or fainter than FLASH level 12 could be slightly under- or over-subtracted. Finally, another effect that would warrant analysis is whether the final science image background has a slight gradient after the reference file is applied to science data. This could be caused by a mismatch of CTE effects between the high signal-to-noise images used to generate the post-flash reference file versus the lower post-flash level used in typical science images. The lower counts will be more affected by charge traps i.e. they will experience a higher level of CTE loss than the higher signal-to-noise images which went into the reference file construction.

Acknowledgements

The authors would like to thank Harish Khandrika for reviewing this ISR and providing valuable feedback. We would also like to thank Dr. Peter McCullough for his input on the

topic of LED fringing and Faizan Naqvi (GSFC) for providing the technical specifications of the WFC3 LED.

References

Anderson,J., Mackenty, J., Baggett, S., and Noeske, K., 2012, "The Efficacy of Post-Flashing for Mitigating CTE-Losses in WFC3/UVIS Images," unpublished white paper.

Baggett, S., and Wheeler, T., 2012, "WFC3/UVIS TV Post-flash Results," TIR WFC3 2012-01. Biretta, J., and Baggett, S., 2013, "WFC3 Post-Flash Calibration" ISR WFC3 2013-12.

Deustua, S, ed. 2016, "WFC3 Data Handbook", Version 3.0, (Baltimore: STScI).

Gosmeyer, K., and Baggett, S., 2017, "WFC3/UVIS External CTE Monitor: 2016 Updates on Coeffcients and Analysis Pipeline" ISR WFC3 2017-09.

Kurtz, H. and Sabbi, E., "UVIS Fringing Removal", WFC3 ISR 2017 In Prep.

Martlin, C., and Baggett, S., 2017, "Longterm Stability of the Post-Flash LED Lamp," ISR WFC3 2017-03

Naqvi, F., 2016, priv.comm.

'OptoDiode Optoelectronics Data Book'. Publication. Opto Diode Corporation, 2015. Web. 15 May 2017. $http://optodiode.com/pdf/ODC_Catalog.pdf$.

Platais, V., 2014, Astrometric Correction for WFC3/UVIS Filter-Dependent Component of Distortion, ISR WFC3 2014-12.

Russell, R., Deustua, S., Anderson, J., Baggett, S.M., Bajaj, V., Bourque, M., Bowers, A., Dahlen, D., Durbin, M., Gosmeyer, C., Gunning, H., Khandrika, H., Mack, J., MacKenty, J., Martlin, C., Kozhurina-Platais, V., Sabbi, E., and Sosey, M., The Updated Calibration Pipeline for WFC3/UVIS: A Reference Guide to Calwf3 3.3, ISR WFC3 2016-01.

Wong, M.H., 2010, "Amplitude of fringing in WFC3/UVIS narrowband red filters", WFC3 ISR WFC3 2010-04